Solvent vapor annealing for controlled pore expansion of block copolymer-assembled inorganic mesoporous films.

Alberto Alvarez-Fernandez,[†] Maximiliano Jara Fornerod,[†] Barry Reid,[†] and Stefan Guldin[†,]*

[†]Department of Chemical Engineering, University College London, Torrington Place, London, WC1E 7JE, UK

E-mail: s.guldin@ucl.ac.uk

Abstract

Mesoporous inorganic thin films are promising materials architectures for a variety of high-value applications, ranging from optical coatings and purification membranes to sensing and energy storage devices. Having precise control over the structural parameters of the porous network is crucial for expanding their applicability. To this end, the use of block copolymers (BCP) as sacrificial structure-directing agents via micelle co-assembly is a particularly attractive route, since the resultant pore size is directly related to scaling laws for the radius of gyration of the pore-forming macromolecule. However, tailoring the molecular weight of the BCP via bespoke synthesis is an elaborate process that requires precise control over highly sensitive reactions conditions. Alternative methods have emerged, based on supramolecular assembly or the addition of different swelling

agents, but, to-date, these present a negative impact on the structural order and pore size dispersity of the final inorganic mesoporous films. In this work, we propose a novel and effective method for control over pore size, porosity and structural order, which relies on a synergistic combination of BCP selective swelling via solvent vapor annealing (SVA) and locking of the structure by condensation of the inorganic sol-gel precursors. The results obtained in this work for TiO_2 establish SVA as a new, straightforward, simple, and powerful route for the fabrication of mesoporous thin-film materials with controllable structural characteristics.

Introduction

Mesoporous architectures with pores on the 5-50 nm length scale offer distinct opportunities for a wide range of applications, such as energy conversion and storage devices,[1–3] separation and purification membranes,[4,5] chemical/bio-sensors,[6,7] or optical coatings.[8,9] Having precise control over the mesoporous structural parameters, i.e. pore size, pore arrangement and overall porosity constitutes in many use cases an important requirement. [10,11]

Bottom-up fabrication strategy based on the use of sacrificial structure-directing agents (SDAs) has proven a particularly attractive method to create ordered mesoporous thin films with tunable pore size and porosity.[12–15] Following this approach, SDAs interact with inorganic precursors (typically sol-gel derived) via preferential supramolecular interactions in solution. In a subsequent step, hybrid composites are produced via evaporation-induced co-assembly and transformed into an ordered inverse opal-type mesoporous structure by thermal calcination or other chemical degradation processes.[16,17] While small surfactant molecules are suitable sacrificial blocks for the fabrication of 2-5

nm pore size mesoporous structures,[18,19] the use of block copolymers (BCPs) as SDA constitutes a versatile, straightforward, cost-effective, and reliable method for the fabrication of larger pore size architectures (8-50nm).[20–22] In the case of BCP co-assembly, the final mesoporous structure can be easily tuned by controlling the macromolecular characteristics of the starting BCP, i.e. the degree of polymerization (N) and mixing ratio between BCP and inorganic precursors. While pore size is commonly determined by the molecular weight of the pore-forming segment of the BCP, control over the mixing ratio, allows the fine-tuning of the total porosity of the sample.[23–25] Therefore, the synthesis of BCPs with well-defined molecular weight for each of the blocks is imperative for precise control over the resulting mesoporous films. However, the tailored synthesis of BCP constitutes a challenging and elaborate process that often involves multiple purification steps, precise reaction conditions, and controlled atmosphere procedures, limiting overall the implementation of this approach as a standard method for tailoring the pore size.[26,27]

Extensive research has been carried out in the last decade in the search for alternative and complementary methods for limiting the synthetic effort necessary for continuous pore tuning and nanostructure optimization. One approach introduced by our group is size exclusion chromatographic fractionation of polydisperse BCPs, which may serve for systematic pore size control and reduction of dispersity of the resulting mesoporous inorganic thin film architectures.[28] Alternative methods based on pore expansion by supramolecular co-assembly of swelling agents, carefully chosen to selectively interact with the pore-forming block, have been successfully implemented. To this end, benzene derivatives,[29,30] homopolymers,[31,32] carboxylic acids,[33,34], or solvents such as toluene or xylene[35,36] have been used for tuning structural dimensions of the final inorganic mesoporous thin film. However, following this approach, and contrary to the size

exclusion chromatography, a negative impact in pore size dispersity and long-range order of the structure has been identified.[37] Moreover, macroscopic phase separation at large swelling agent – BCP ratios limits its application for continuous pore tuning. Therefore, the search for simple, fast, and scalable approaches that allow for continuous pore tuning remains a challenging research endeavor.

To this end, solvent vapor annealing (SVA) constitutes an interesting approach. SVA is a widely used technique in the BCP nanolithography field for controlling both, the final BCP morphology and the microstructure orientation in thin-film configuration.[38–40] During SVA treatments, BCP thin films are exposed to vapors of one (or more) solvent that swell the film and provide mobility to the polymer chains to diffuse and reorganize, promoting the ordering of the BCP structures. However, after a rapid dry quenching, films typically recover their original thickness.[41,42]

In this work, we propose the combination of solvent vapor annealing (SVA) and sol-gel reaction as a promising and effective alternative method for pore expansion on mesoporous thin films. To this end, hybrid films composed of the amphiphilic block copolymer poly(isobutylene)-block-poly(ethylene oxide) (PIB-b-PEO) and TiO_2 sol precursors are swollen by exposing samples to vapors of cyclohexane, a selective solvent for PIB block for a defined amount of time. Concurrently, the swollen structure is locked in place by the condensation reaction of the inorganic precursors, which is followed by Fourier-transform infrared spectroscopy (FTIR). Finally, the mesoporous TiO_2 thin films are characterized by scanning electron microscopy (SEM), atomic force microscopy (AFM) and ellipsometric porosimetry (EP) to fully validate this approach.

Results

Tunable mesoporous structures were obtained following the methodology sketched in **Figure 1**. The pore-forming polymer block, PIB, is swollen by exposing samples to vapors of a selective solvent. Concurrently, the structure is locked in place by the condensation reaction of the inorganic precursors, allowing to have a precise pore size tuning via pore swelling.

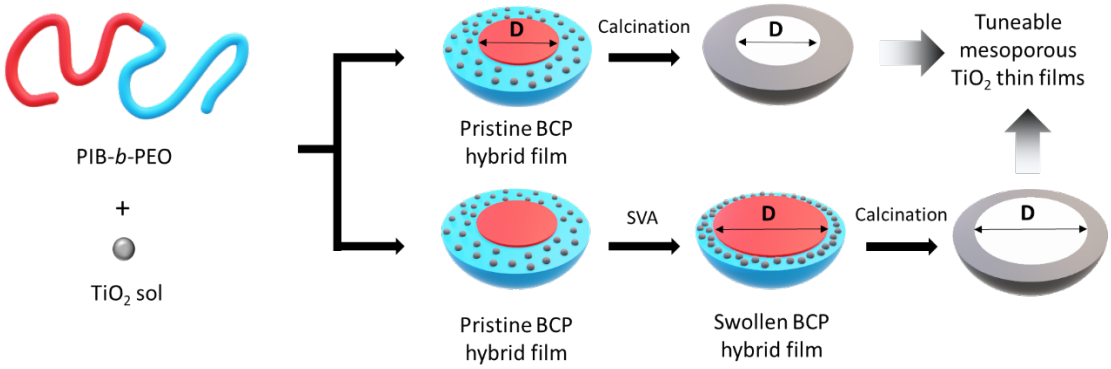

Figure 1. Schematic illustration of the BCP co-assembly swell & lock SVA pore expansion process. Hybrid BCP films are exposed to cyclohexane vapors, with the consequent swelling of the micelle PIB core. After 30 min or 1 h at room temperature, samples are removed and calcined at 450 °C. The partial condensation reaction of the inorganic sol-gel precursors during the SVA process allows tuning the pore size and porosity of the final inorganic structure.

The first critical step is therefore to choose the correct solvent in order to have a selective swelling of the pore-forming block. **Table 2** lists the respective polymer-solvent interaction parameters, calculated using the Hansen solubility values for both BCP blocks (PIB and PEO), and common organic solvents (THF, cyclohexane, and toluene) studied during this work.

Solvent or polymer	δ_d ($MPa^{1/2}$)	δ_p ($MPa^{1/2}$)	δ_h ($MPa^{1/2}$)	V ($\mu m^3\ mol^{-1}$)	V_p (kPa)[a]	$\chi_{pol\text{-}THF}$[b]	$\chi_{pol\text{-}cyclohexane}$[b]	$\chi_{pol\text{-}toluene}$[b]
THF[43]	16.8	5.7	8.0	81.7	23.4	-	-	-
Cyclohexane[44]	16.8	0.00	0.20	108.9	13.1	-	-	-
Toluene[43]	18.0	1.4	2.0	137.1	3.8	-	-	-
PIB[45]	14.5	2.07	4.66	63.3	-	0.29	0.28	0.36
PEO[46]	17.3	3.0	9.4	38.9	-	0.04	0.37	0.23

Table 1. Hansen solubility parameters for the BCP materials studied. [a] Vapor pressures are at 298K. [b] Values of χ parameters are estimated at 298K using: $\chi_{ij} = \frac{V}{RT}[(\delta_{dj} - \delta_{di})^2 + 0.25(\delta_{pj} - \delta_{pi})^2 + 0.25(\delta_{hj} - \delta_{hi})^2]$, where δ_d, δ_p, δ_h are parameters related to dispersion, polarity and hydrogen bonding respectively, V is the molar volume and χ is the Flory-Huggins interaction parameter.

From a consideration of interaction parameters, all screened solvents are suitable solvents for swelling the PIB block ($\chi_{PIB\text{-}solvent} < 0.4$). However, THF exhibits a higher affinity for the PEO block ($\chi_{PIB\text{-}THF} = 0.29$ vs. $\chi_{PEO\text{-}THF} = 0.04$), making it less appropriate for the selective swelling of the PIB micelle core. In this sense, cyclohexane offers more suitable characteristics, since it presents a low interaction parameter with the PIB part while displaying a high interaction parameter with the PEO block, allowing the selective swelling of the former block.

In order to gain further insights into the BCP film swelling process, a pure PIB-*b*-PEO film was deposited on a Si substrate by spin-coating and enclosed in a solvent annealing chamber. Vapors of the three different solvents were consecutively introduced and film thickness was recorded in-situ by ellipsometry. **Figure S1** shows the film swelling after 25 min of SVA for each solvent. In all cases, film thickness increased from the initial 116

nm to 136, 150, and 155 nm using toluene, cyclohexane, or THF respectively. The lower vapor pressure of toluene compared with THF or cyclohexane explains its low swelling ratio, while the low selectivity of the THF is in line with the higher swelling ratios observed. Therefore, and taking into account its low vapor pressure, high selectivity, and high swelling ratios, cyclohexane emerged as the most suitable solvent for selective PIB-*b*-PEO swelling and was used during the subsequent SVA experiments.

To study the swelling behavior of the co-assembled organic-inorganic film, a hybrid BCP:TiO_2 sol solution with a O:I ratio corresponding to α (see experimental part) was deposited onto a silicon wafer and introduced in the SVA chamber. SVA experiments were followed in-situ by ellipsometry in order to monitor the swelling process (**Figure S2**). In a first step (1 in **Figure 2**) N_2 gas was introduced in the chamber in order to stabilize film thickness. After cyclohexane entered the chamber (2 in **Figure 2**), the hybrid film started to swell, reaching a maximum thickness of 245 - 250 nm (from the original 195 nm), which was kept constant during the duration of the SVA treatment. Finally, pure N_2 gas was introduced again in the chamber (3 in **Figure 2**), invoking the film to de-swell. In contrast to purely organic BCP films (**Figure 2A**), in which the original thickness was recovered after solvent removal, hybrid BCP:TiO_2 sol films were able to partially retain their swollen thickness (**Figure 2B**). Interestingly, longer solvent annealing of the hybrid films led to a higher overall thickness at the end of the process (**Figure 2C**).

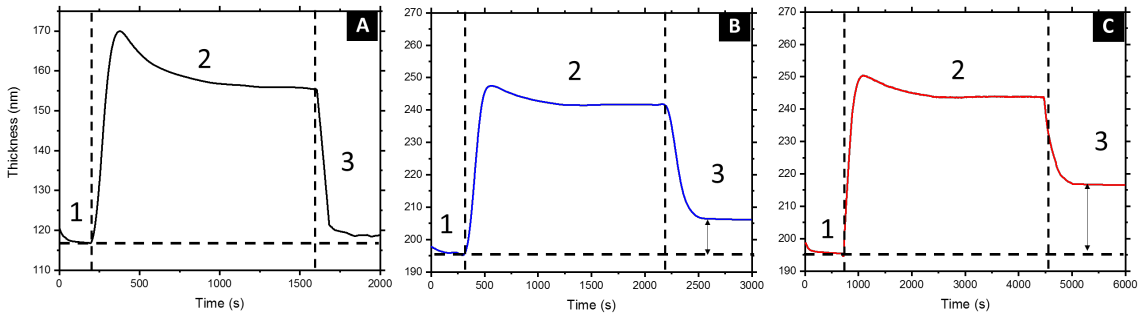

Figure 2. Film thickness evolution profile during the SVA treatment for a pure BCP (25min) (A), and a hybrid BCP:TiO_2 sol thin film (B, 30 min and C, 1h)

The different behavior observed between pure and hybrid BCP film may be explained by taking into account the sol-gel reaction of the inorganic precursors presented in the BCP hybrid micelles. Thus, FTIR measurements were performed at different stages of the process in order to monitor the condensation reaction. **Figure 3A** shows the FTIR spectra of the hybrid samples (*i.e.* before final calcination) at different times: t = 0 min (reference), and after 30 min and 1 hour SVA respectively. All spectra present similar bands: a broad band around 3250 cm^{-1}, which is attributed to the O-H stretching mode of Ti-OH groups, a sharp peak centered around 2800 cm^{-1} corresponding to the C-H stretch of the polymeric chains, and a band at 800 cm^{-1} due to the Ti-O bond stretching mode.

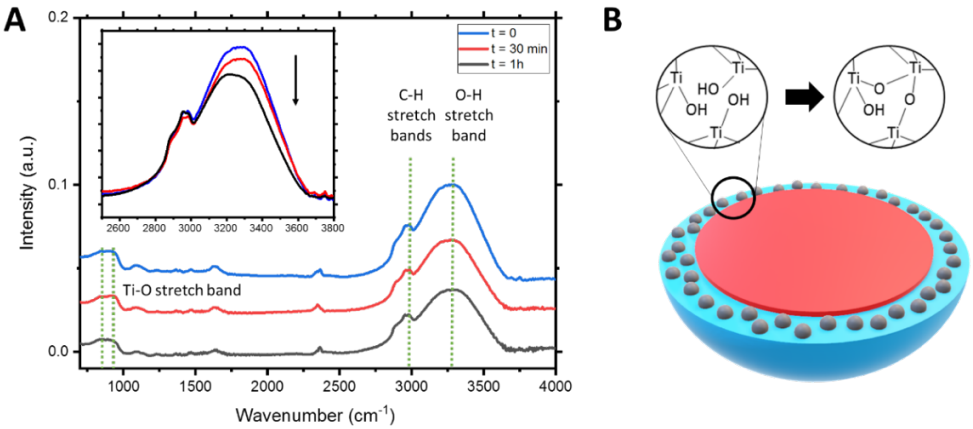

Figure 3. A) FTIR spectra of the hybrid BCP samples before (black line) and after (red and blue line) SVA. B) Schematic representation of the partial condensation reaction that takes place in the shell of the micelle during the SVA process.

Interestingly, a direct comparison of all spectra in the 2500 – 3800 cm^{-1} area (see inset in **Figure 3A**) shows a clear reduction in the O-H band intensity during the SVA, suggesting a partial condensation reaction of the Ti-OH sol precursors located at the micelle shell (**Figure 3B**). This partial reaction is due to the spontaneous condensation of the hydroxo-Ti complex formed during the hydrolysis of the Ti precursors.[47] In the case of the BCP-Ti hybrid films, this condensation reaction, even if not completed, provides enough mechanical strength to the swollen structure to retain in an expanded state after the sample is removed from the SVA chamber (**Figure 2B-C**). In contrast, when pure BCP film, i.e., with no inorganic sol, is exposed to the SVA, the polymer film recovers its original thickness once removed from the chamber, as previously reported for BCP SVA systems.[48]

In order to study the effect of the SVA in the final inorganic mesoporous structure, hybrid samples were calcined in a furnace for the complete removal of the BCP. **Figure 4A-C** shows a comparison of the topographical AFM micrographs for the corresponding mesoporous TiO_2 films. A clear enlargement of the pore structure can be detected as a result of the selective film swelling and structural locking during the SVA treatment. In order to gain more insights into the porous characterization of the mesoporous architectures, the average pore diameter was determined by analysis of the real space topography images using the Pebbles software (**Figure S3**). Pore size distribution histograms show a clear evolution of the structure during the annealing process with pore size diameter (D) increasing from D = 8.2 ± 1.7 nm (t = 0), to D = 9.9±2.5 (t = 30min) and D = 13.9±2.0 nm (t = 1h) respectively (**Figure 4D-F**). It is important to mention here that longer annealing times (1.5h) did not result in a continuation of this trend. As presented in the Supporting Information (**Figure S4**), AFM topographical micrography

showed a gradual loss of the highly ordered structure. While the majority of pores displayed diameters of around 15 nm, bigger pores with D > 50 nm started appearing, indicating polymer rearrangement and reconstruction of the micelle packing, an unwanted effect in this context that enhanced pore dispersity. Therefore, SVA annealing times were limited in the following to 1h.

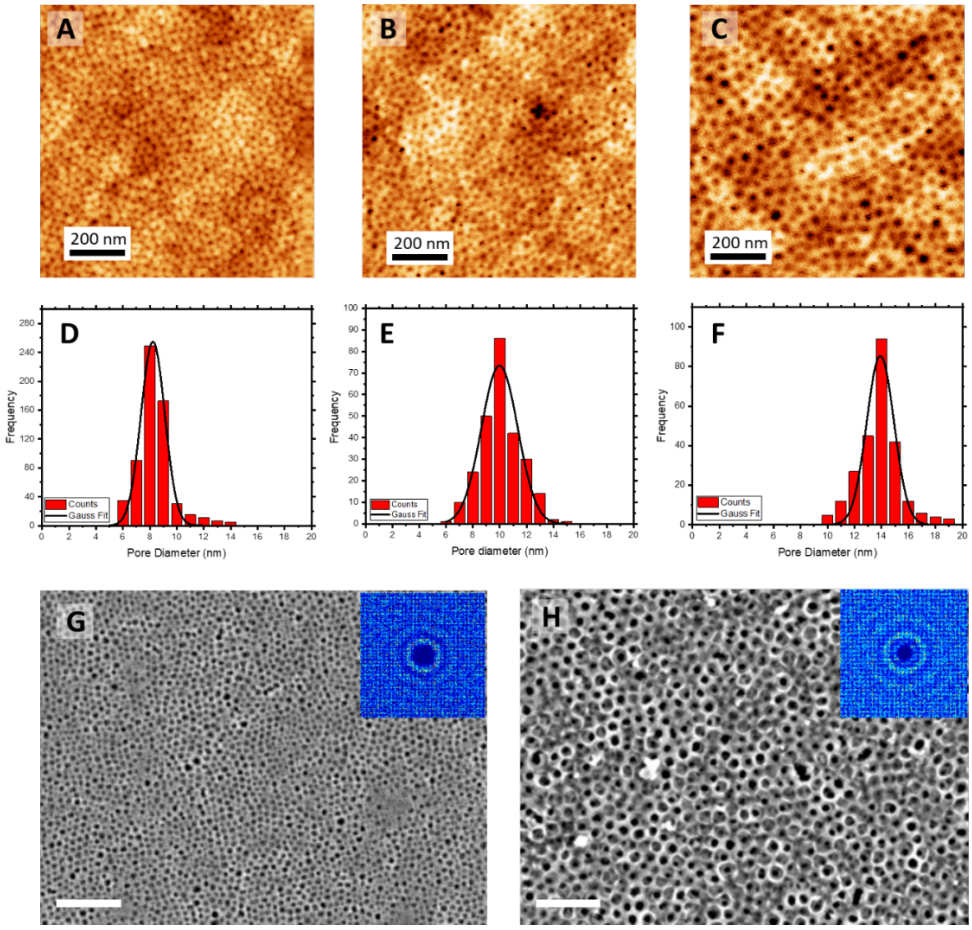

Figure 4. AFM topographical images of the TiO_2 mesoporous films (α, α*) obtained with no SVA (A) and after 30 min (B) and 1 h (C) SVA treatment respectively. Corresponding pore diameter histograms obtained by image analysis (D-F). SEM images of the TiO_2 mesoporous films with no SVA (G) and after 1 h SVA treatment (H). The inset corresponds to the 2D spatial distribution function to evaluate pore ordering. Scale bar: 150 nm.

As previously introduced, one major limitations of swelling agents to-date is their negative impact on the structural order and pore size dispersity of the final inorganic films. In this sense, our approach is able to overpass this limitation through a combination of film swelling by SVA and locking of the swollen structure by inducing the condensation reaction of the inorganic precursors, **Figure 4G-H** shows the SEM micrographs of the mesoporous TiO_2 films obtained with and without SVA treatment. In line with previous AFM measurements, a clear enlargement of the porous structure can be detected. SEM micrographs were analyzed using CORDERLY [49] (an alternative software to the standard 2D fast Fourier transform (FFT)), to evaluate the impact of the SVA treatment on the mesoporous arrangement of the samples. The higher number of concentric hexagonal rings displayed in the 2D spatial distribution function (SDF) (insets **Figure 4G-H)** of the sample exposed to the SVA treatment suggests a higher degree of order compared to the non-treated sample, which provides a further advantage of the approach.

To confirm the critical role of the sol-gel condensation reaction in the process to lock the structure, an alternative sol with lower reactivity was also explored during this work. Hybrid BCP - aluminosilicate sol films were prepared and exposed to the same SVA experimental conditions as TiO_2 films. **Figure S5A-B** shows the AFM micrographs of the aluminosilicate mesoporous films obtained after calcination. While an improvement in the structural order can also be detected in this case, no clear impact in the pore size distribution or porosity was observed (**Figure S5C-D**). While for previous TiO_2 hybrid films a partial spontaneous condensation reaction was detected, FTIR spectra of the hybrid aluminosilicate films present identical intensities before and after the SVA treatment (**Figure S5E**). The absence of spontaneous condensation reaction prevents any

pore expansion effect. These results highlight the importance of the sol-gel condensation reaction in providing the necessary structural integrity to the hybrid film to retain a pore enlargement after SVA.

Previous works have put AFM and SEM in context to other techniques for a precise structural characterization of mesoporous thin films, showing their limitations in providing essential structural information such as out-of-plane pore dimensions and spacing nor porosity.[20] Thus, for a more complete view, samples were also analyzed by ellipsometric porosimetry (EP). **Figure 5A-C** shows the adsorption isotherm for the studied samples. A clear change in the total porosity of the sample was observed with the SVA treatment (29 vs. 48 % after 1 h SVA in cyclohexane). Moreover, further analysis of the EP adsorption isotherms using Kelvin equation allowed obtaining the pore radius distribution of the mesoporous thin films. While untreated samples (α) exhibited a pore size diameter D = 8.9 ± 1.5 nm (**Figure 5D**), identical samples exposed 1 h to cyclohexane vapor (α*) presented a D = 14.8 ± 1.9 nm (**Figure 5F**). These results confirm the controlled expansion of the inorganic structure after the swelling and locking SVA procedure. An intermediate result with D = 10.3± 2.1 nm (**Figure 5B** and **5E**), was observed for a shorter SVA treatment (30 min), demonstrating the possibility of tuning the structural parameters by the length of the SVA treatment.

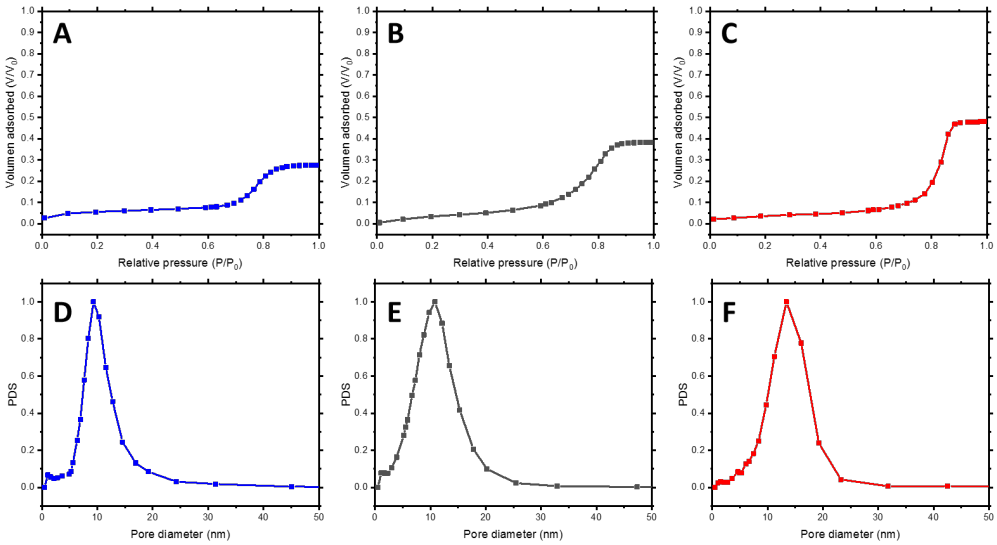

Figure 5. EP adsorption isotherms (A-C) with correlated pore size distributions (D-F) for the non-treated film (A, D), 30 min cyclohexane SVA (B, E), and 1 h cyclohexane SVA (C, F).

In order to study the effect of the inorganic content in the final structure obtained after SVA, samples with increasing O:I ratios were exposed 1 h to cyclohexane vapors. **Figure 6A-B** shows the EP adsorption isotherms for β and γ samples respectively. In both cases, the increment in the organic content in the starting hybrid solution allows increasing the original porosity of non-treated samples (42 and 58% respectively), compared with the 29% observed for α (**Figure 5A**). This is in line with previous observations, where total porosity values are controlled by the O:I ratio.[12] We consistently measured a higher porosity after the SVA for films with all the different O:I ratios. Thus, final porosity retained for β* samples increased from 42% to 59% and for γ* from 58% to 70% with the SVA (**Figure 6A-B**).

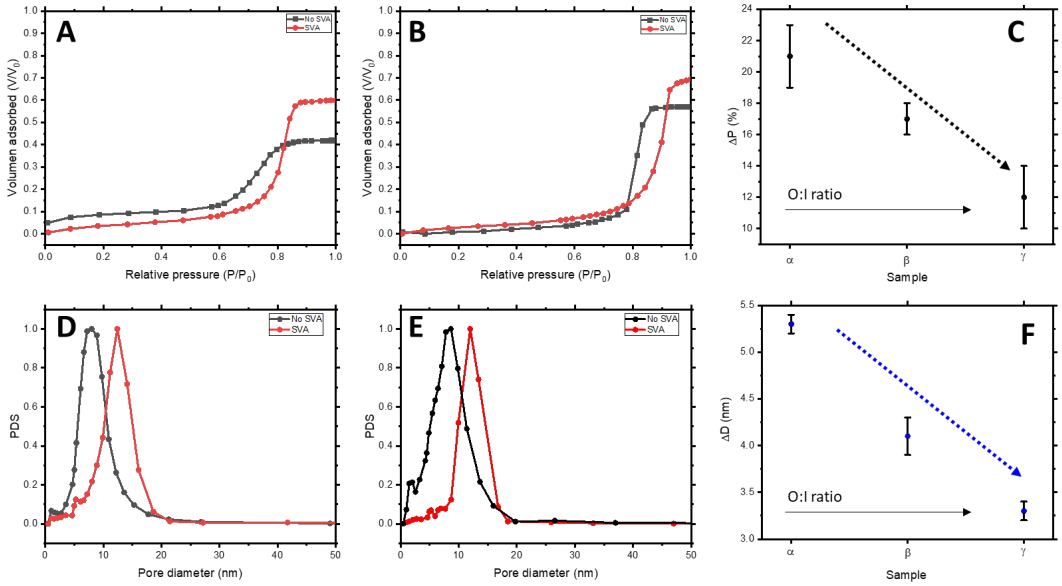

Figure 6. EP adsorption isotherms (top) with correlated pore size distributions (bottom) for different O:I ratios: β (A, D) and γ (B, E) with (red line) and without (black line) SVA. Effect of the SVA process over porosity (C) and pore diameter (F) for the three different O:I ratios presented in this work (α, β, and γ respectively).

Non-treated α, β, and γ samples presented very similar pore sizes, with values ranging from 8.9± 1.5 to 8.3±1.6 and 8.6±1.8 nm, respectively. However, a notable difference in pore sizes was observed after the SVA treatment. The sample with the lower O:I ratio (α*) increased the pore size from D = 8.9 ± 1.5 nm to D = 14.8 ± 1.9 nm with the SVA, as previously discussed. Increasing the O:I ratio (β*) led to a pore size of D = 12.4 ± 2.0 nm, while D values for higher O:I ratio (γ*) reached D = 11.9 ± 1.9 nm respectively. In addition to the clear pore size increment due to the SVA, another tendency can be extracted with the systematic change in the O:I ratio: the ability of the condensation reaction to lock the swollen structure is proportional to the inorganic content in the hybrid solution (**Figure 6C** and **6F**). We relate this trend to the higher structural integrity of the partially condensed Ti network obtained with higher inorganic content. These results

establish the combination of vapor swelling and sol-gel locking as a new and versatile approach for controllable expansion of inorganic mesoporous thin films.

Conclusion

In this work, we establish solvent vapor annealing (SVA) as a new and straightforward approach for tuning the pore size and porosity in TiO_2 mesoporous thin film architectures fabricated by the co-assembly of block copolymers with sol-gel precursors. The approach relies on a synergistic interplay between dimensional tuning by selective solvent swelling of the pore-forming BCP block and the spontaneous condensation of the inorganic matrix. A complete library of TiO_2 mesoporous coatings with different porosity and pore sizes was obtained by exposing organic-inorganic hybrid films to cyclohexane vapors for 30 min and 1 h. The combination of structural characterization by AFM, SEM, and EP and the chemical information obtained by FTIR allowed the establishment of a close relationship between the sol-gel condensation reaction and the final expansion of the mesoporous structure obtained after SVA. Moreover, a clear enhancement in the long-range order of the final inorganic mesoporous structure was found as a result of the SVA treatment. These results highlight the relevance and versatility of the SVA as a new standard method for the controllable expansion of mesoporous thin films.

Experimental Section/

Reagents: $PIB_{3.9}$-*b*-$PEO_{3.6}$ block copolymer (polydispersity 1.26, Mn 4.85 kg mol^{-1}) was provided by BASF. Toluene (99.9%), 1-butanol (99.4%), hydrochloric acid (HCl, fuming 37%) and Titanium isopropoxide (TiOPr, >98%) were purchased from Merk. All chemicals were used without further purification.

Preparation of mesoporous TiO_2 films: $PIB_{3.9}$-b-$PEO_{3.6}$ BCP (Mn 4.85 kg/mol; polydispersity index (PDI) 1.26) was supplied by BASF following previously reported synthetic route.[50] Inorganic sol material and mesoporous inorganic TiO_2 films were prepared as described in previous works[8,16]. Thus, a 50 mg/ml BCP solution was prepared using toluene/1-butanol azeotrope (72.84/27.16 wt%) as solvent. TiO_2 inorganic sol was prepared by the addition of 0.193ml of TiOPr to a 0.061mL of HCl, under continuous stirring. In a final step different organic-inorganic (O:I) ratio solutions were prepared as described in **Table 1**. All samples were deposited by spin-coating on 1x1 cm silicon substrates at 2000 rpm for 30 seconds. Immediately after the film deposition, samples were introduced in the solvent vapor annealing (SVA) chamber (**Figure S2A**). Solvent-rich atmosphere inside the chamber was created by the continuous stream of a toluene, THF or cyclohexane vapors produced by bubbling nitrogen gas (0.1 l/min-1, flow controller F-201CV, Bronkhorst) through the corresponding liquid solvent. SVA treatments were carried out for up to 1 h at room temperature (22 °C). Finally, and to remove the BCP, samples, were calcined in a muffle furnace at 450 °C for 30 min.

Sample	Volume of TiO_2 (ml)	Volume of HCl (ml)	BCP solution volume (ml)
α / α *	0.193	0.061	0.650
β / β *	0.193	0.061	1
γ / γ *	0.193	0.061	1.250

Table 2. List of samples that were studied during this work. * SVA sample

Samples characterization: AFM images were obtained on a Bruker Dimension Icon atomic force microscope with a Bruker ScanAsyst Air probe (nominal tip radius 2 nm) in

tapping mode**.** The average pore radius was determined by analysis of the real space topography images using the Pebbles software[51].

SEM images were taken in a Xbeam 540 FIB/SEM (ZEISS) directly on TiO_2 mesoporous films without any metallic coating. Images were captured using an acceleration voltage between 0.5 to 2 kV and working distance between 0.9 to 1 mm. The 2D spatial distribution function was calculated with the software CORDERLY.[49]

Ellipsometric porosimetry (EP) measurements were carried out on a Semilab SE2000 variable angle spectroscopic ellipsometer in the spectral range of 300 to 1000 nm. All data analysis was performed using the Semilabs SEA software (v1.6.2). Before EP measurements, samples were placed on a hotplate at 120 °C for 10 minutes to remove residual atmospheric water molecules inside the pores. Fourier-transform infrared spectroscopy (FTIR) measurements of the samples before and after the SVA step were performed using a AIM-9000 infrared microscope coupled with IRTracer-1000 FTIR spectrophotometer (Shimadzu) in reflection mode. Atmospheric and baseline correction were performed with the software Lab Solutions IR (Shimadzu). In order to increase the sample reflectance, gold-coated Si substrates were used during this study.

Supporting Information

The Supporting Information is available free of charge on the ACS Publications website at DOI: 10.1021/acs.langmuir.XXXXXXX.

- In-situ ellipsometry of film swelling for purely organic block copolymer samples in various solvents.
- Information of the experimental set-up used for SVA.
- Evidence of the image analysis used for pore size determination.
- AFM micrograph of mesoporous film after 1.5h of SVA.

- Experimental data (AFM, ellipsometric porosimetry, FTIR) for aluminosilicate samples.

Acknowledgments

AAF, MJF, and SG acknowledge funding by EPSRC New Investigator Award (EP/R035105/1). MJF is grateful for support of the Henry Royce Institute through the Royce PhD Equipment Access Scheme enabling access to microscopy facilities at Royce@Cambridge; EPSRC Grant Number EP/R00661X/1. BR was supported by an EPSRC Industrial Case Award (EP/M506448/1) in support of BASF.

References

(1) Eftekhari, A. Ordered Mesoporous Materials for Lithium-Ion Batteries. *Microporous and Mesoporous Mater.* **2017**, *243*, 355–369. https://doi.org/10.1016/j.micromeso.2017.02.055.

(2) Li, W.; Liu, J.; Zhao, D. Mesoporous Materials for Energy Conversion and Storage Devices. *Nat. Rev. Mater.* **2016**, *1* (6), 16023. https://doi.org/10.1038/natrevmats.2016.23.

(3) Du, G.; Xu, Y.; Zheng, S.; Xue, H.; Pang, H. The State of Research Regarding Ordered Mesoporous Materials in Batteries. *Small* **2019**, *15* (11), 1804600. https://doi.org/10.1002/smll.201804600.

(4) Yang, J.; Lin, G. S.; Mou, C. Y.; Tung, K. L. Mesoporous Silica Thin Membrane with Tunable Pore Size for Ultrahigh Permeation and Precise Molecular Separation. *ACS Appl. Mater. Interfaces* **2020**, *12* (6), 7459–7465. https://doi.org/10.1021/acsami.9b21042.

(5) Jang, K. S.; Kim, H. J.; Johnson, J. R.; Kim, W. G.; Koros, W. J.; Jones, C. W.; Nair, S. Modified Mesoporous Silica Gas Separation Membranes on Polymeric Hollow Fibers. *Chem. Mater.* **2011**, *23* (12), 3025–3028. https://doi.org/10.1021/cm200939d.

(6) Yang, X.; Qiu, P.; Yang, J.; Fan, Y.; Wang, L.; Jiang, W.; Cheng, X.; Deng, Y.; Luo, W. Mesoporous Materials–Based Electrochemical Biosensors from Enzymatic to Nonenzymatic. *Small* **2021**, *17* (9), 1904022. https://doi.org/10.1002/smll.201904022.

(7) Bearzotti, A.; Bertolo, J. M.; Innocenzi, P.; Falcaro, P.; Traversa, E. Humidity Sensors Based on Mesoporous Silica Thin Films Synthesised by Block Copolymers. *J. Eur. Ceram. Soc.* **2004**, *24* (6), 1969–1972. https://doi.org/10.1016/S0955-2219(03)00521-1.

(8) Reid, B.; Taylor, A.; Chen, Y.; Schmidt-Hansberg, B.; Guldin, S. Robust Operation of Mesoporous Antireflective Coatings under Variable Ambient Conditions. *ACS App. Mater. Interfaces* **2018**, *10* (12), 10315–10321. https://doi.org/10.1021/acsami.7b18299.

(9) Guldin, S.; Kohn, P.; Stefik, M.; Song, J.; Divitini, G.; Ecarla, F.; Ducati, C.; Wiesner, U.; Steiner, U. Self-Cleaning Antireflective Optical Coatings. *Nano Letters* **2013**, *13* (11), 5329–5335. https://doi.org/10.1021/nl402832u.
(10) Nagy, E. *Basic Equations of Mass Transport Through a Membrane Layer*; Elsevier, 2019. https://doi.org/10.1016/C2016-0-04043-3.
(11) Walcarius, A. Mesoporous Materials-Based Electrochemical Sensors. *Electroanalysis* **2015**, *27* (6), 1303–1340. https://doi.org/10.1002/elan.201400628.
(12) Lokupitiya, H. N.; Jones, A.; Reid, B.; Guldin, S.; Stefik, M. Ordered Mesoporous to Macroporous Oxides with Tunable Isomorphic Architectures: Solution Criteria for Persistent Micelle Templates. *Chem. Mater.* **2016**, *28* (6), 1653–1667. https://doi.org/10.1021/acs.chemmater.5b04407.
(13) Grosso, D.; Cagnol, F.; Soler-Illia, G. J. de A. A.; Crepaldi, E. L.; Amenitsch, H.; Brunet-Bruneau, A.; Bourgeois, A.; Sanchez, C. Fundamentals of Mesostructuring Through Evaporation-Induced Self-Assembly. *Adv. Funct. Mater.* **2004**, *14* (4), 309–322. https://doi.org/10.1002/adfm.200305036.
(14) Stefik, M.; Guldin, S.; Vignolini, S.; Wiesner, U.; Steiner, U. Block Copolymer Self-Assembly for Nanophotonics. *Chem. Soc. Rev.* **2015**, *44* (15), 5076–5091. https://doi.org/10.1039/c4cs00517a.
(15) Alberius, P. C. A.; Frindell, K. L.; Hayward, R. C.; Kramer, E. J.; Stucky, G. D.; Chmelka, B. F. General Predictive Syntheses of Cubic, Hexagonal, and Lamellar Silica and Titania Mesostructured Thin Films. *Chem. Mater.* **2002**, *14* (8), 3284–3294. https://doi.org/10.1021/cm011209u.
(16) Reid, B.; Taylor, A.; Alvarez-Fernandez, A.; Ismael, M. H.; Sharma, S.; Schmidt-Hansberg, B.; Guldin, S. Photocatalytic Template Removal by Non-Ozone-Generating UV Irradiation for the Fabrication of Well-Defined Mesoporous Inorganic Coatings. *ACS App. Mater. Interfaces* **2019**, *11* (21), 19308–19314. https://doi.org/10.1021/acsami.9b01199.
(17) Guldin, S.; Hüttner, S.; Tiwana, P.; Orilall, M. C.; Ülgüt, B.; Stefik, M.; Docampo, P.; Kolle, M.; Divitini, G.; Ducati, C.; Redfern, S. A. T.; Snaith, H. J.; Wiesner, U.; Eder, D.; Steiner, U. Improved Conductivity in Dye-Sensitised Solar Cells through Block-Copolymer Confined TiO 2 Crystallisation. *Energy Environ. Sci.* **2011**, *4* (1), 225–233. https://doi.org/10.1039/C0EE00362J.
(18) Park, K. W.; Kim, J. Y.; Seo, H. J.; Kwon, O. Y. Preparation of Mesoporous Silica by Nonionic Surfactant Micelle–Templated Gelation of Na2SiO3 and H2SiF6 and Application as a Catalyst Carrier for the Partial Oxidation of CH4. *Sci. Rep.* **2019**, *9* (1), 1–8. https://doi.org/10.1038/s41598-019-50053-y.
(19) Walcarius, A.; Sibottier, E.; Etienne, M.; Ghanbaja, J. Electrochemically Assisted Self-Assembly of Mesoporous Silica Thin Films. *Nat. Mater.* **2007**, *6* (8), 602–608. https://doi.org/10.1038/nmat1951.
(20) Alvarez-Fernandez, A.; Reid, B.; Fornerod, M. J.; Taylor, A.; Divitini, G.; Guldin, S. Structural Characterization of Mesoporous Thin Film Architectures: A Tutorial Overview. *ACS App. Mater. Interfaces* **2020**, *12* (5), 5195–5208. https://doi.org/10.1021/acsami.9b17899.
(21) Nedelcu, M.; Lee, J.; Crossland, E. J. W.; Warren, S. C.; Orilall, M. C.; Guldin, S.; Hüttner, S.; Ducati, C.; Eder, D.; Wiesner, U.; Steiner, U.; Snaith, H. J. Block Copolymer Directed Synthesis of Mesoporous TiO2 for Dye-Sensitized Solar Cells. *Soft Matter* **2009**, *5* (1), 134–139. https://doi.org/10.1039/b815166k.
(22) Alberti, S.; Steinberg, P. Y.; Giménez, G.; Amenitsch, H.; Ybarra, G.; Azzaroni, O.; Angelomé, P. C.; Soler-Illia, G. J. A. A. Chemical Stability of Mesoporous Oxide Thin Film Electrodes under Electrochemical Cycling: From Dissolution to

Stabilization. *Langmuir* **2019**, *35* (19), 6279–6287. https://doi.org/10.1021/acs.langmuir.9b00224.
(23) Noolandi, J.; Hong, K. M. Theory of Block Copolymer Micelles in Solution. *Macromolecules* **1983**, *16* (9), 1443–1448. https://doi.org/10.1021/ma00243a007.
(24) Templin, M.; Franck, A.; Du Chesne, A.; Leist, H.; Zhang, Y.; Ulrich, R.; Schädler, V.; Wiesner, U. Organically Modified Aluminosilicate Mesostructures from Block Copolymer Phases. *Science* **1997**, *278* (5344), 1795–1798. https://doi.org/10.1126/science.278.5344.1795.
(25) Bloch, E.; Llewellyn, P. L.; Phan, T.; Bertin, D.; Hornebecq, V. On Defining a Simple Empirical Relationship to Predict the Pore Size of Mesoporous Silicas Prepared from PEO-b-PS Diblock Copolymers. *Chem. Mater.* **2009**, *21* (1), 48–55. https://doi.org/10.1021/cm801978w.
(26) Hadjichristidis, N.; Pitsikalis, M.; Iatrou, H. Synthesis of Block Copolymers. In *Block Copolymers I*; Springer-Verlag: Berlin/Heidelberg, 2005; Vol. 189, pp 1–124. https://doi.org/10.1007/12_005.
(27) Uhrig, D.; Mays, J. W. Experimental Techniques in High-Vacuum Anionic Polymerization. *J. Polym. Sci. Part A: Polym. Chem.* **2005**, *43* (24), 6179–6222. https://doi.org/10.1002/pola.21016.
(28) Alvarez-Fernandez, A.; Reid, B.; Suthar, J.; Choy, S. Y.; Jara Fornerod, M.; mac Fhionnlaoich, N.; Yang, L.; Schmidt-Hansberg, B.; Guldin, S. Fractionation of Block Copolymers for Pore Size Control and Reduced Dispersity in Mesoporous Inorganic Thin Films. *Nanoscale* **2020**, *12* (35), 18455–18462. https://doi.org/10.1039/D0NR05132B.
(29) Yi, J.; Kruk, M. Pluronic-P123-Templated Synthesis of Silica with Cubic Ia3d Structure in the Presence of Micelle Swelling Agent. *Langmuir* **2015**, *31* (27), 7623–7632. https://doi.org/10.1021/acs.langmuir.5b01182.
(30) Fan, J.; Yu, C.; Lei, J.; Zhang, Q.; Li, T.; Tu, B.; Zhou, W.; Zhao, D. Low-Temperature Strategy to Synthesize Highly Ordered Mesoporous Silicas with Very Large Pores. *J. Am. Chem. Soc.* **2005**, *127* (31), 10794–10795. https://doi.org/10.1021/ja052619c.
(31) Reid, B.; Alvarez-Fernandez, A.; Schmidt-Hansberg, B.; Guldin, S. Tuning Pore Dimensions of Mesoporous Inorganic Films by Homopolymer Swelling. *Langmuir* **2019**, *35* (43), 14074–14082. https://doi.org/10.1021/acs.langmuir.9b03059.
(32) Sarkar, A.; Thyagarajan, A.; Cole, A.; Stefik, M. Widely Tunable Persistent Micelle Templates: Via Homopolymer Swelling. *Soft Matter* **2019**, *15* (26), 5193–5203. https://doi.org/10.1039/c9sm00484j.
(33) Alvarez-Fernandez, A.; Valdes-Vango, F.; Martín, J. I.; Vélez, M.; Quirós, C.; Hermida-Merino, D.; Portale, G.; Alameda, J. M.; García Alonso, F. J. Tailoring Block Copolymer Nanoporous Thin Films with Acetic Acid as a Small Guest Molecule. *Polym. Int.* **2019**, *68* (11), 1914–1920. https://doi.org/10.1002/pi.5901.
(34) Álvarez-Fernández, A.; Valdés-Bango, F.; Losada-Ambrinos, R.; Martín, J. I.; Vélez, M.; Alameda, J. M.; García Alonso, F. J. Polymer Porous Thin Films Obtained by Direct Spin Coating. *Polym. Int.* **2018**, *67* (4), 393–398. https://doi.org/10.1002/pi.5519.
(35) Li, Y.; Kruk, M. Single-Micelle-Templated Synthesis of Hollow Silica Nanospheres with Tunable Pore Structures. *RSC Adv.* **2015**, *5* (85), 69870–69877. https://doi.org/10.1039/c5ra13492g.
(36) Huang, L.; Kruk, M. Versatile Surfactant/Swelling-Agent Template for Synthesis of Large-Pore Ordered Mesoporous Silicas and Related Hollow Nanoparticles. *Chem. Mat.* **2015**, *27* (3), 679–689. https://doi.org/10.1021/cm5028749.

(37) Wu, Q. L.; Rankin, S. E. Tuning the Mesopore Size of Titania Thin Films Using a Polymeric Swelling Agent. *J. Phys. Chem. C* **2011**, *115* (24), 11925–11933. https://doi.org/10.1021/jp2021193.
(38) Sinturel, C.; Vayer, M.; Morris, M.; Hillmyer, M. A. Solvent Vapor Annealing of Block Polymer Thin Films. *Macromolecules* **2013**, *46* (14), 5399–5415. https://doi.org/10.1021/ma400735a.
(39) Jung, Y. S.; Ross, C. A. Solvent-Vapor-Induced Tunability of Self-Assembled Block Copolymer Patterns. *Adv. Mater.* **2009**, *21* (24), 2540–2545. https://doi.org/10.1002/adma.200802855.
(40) Jin, C.; Olsen, B. C.; Luber, E. J.; Buriak, J. M. Nanopatterning via Solvent Vapor Annealing of Block Copolymer Thin Films. *Chem. Mater.* **2017**, *29* (1), 176–188. https://doi.org/10.1021/acs.chemmater.6b02967.
(41) Posselt, D.; Zhang, J.; Smilgies, D.-M.; Berezkin, A. v.; Potemkin, I. I.; Papadakis, C. M. Restructuring in Block Copolymer Thin Films: In Situ GISAXS Investigations during Solvent Vapor Annealing. *Prog. Polym. Sci.* **2017**, *66*, 80–115. https://doi.org/10.1016/j.progpolymsci.2016.09.009.
(42) Bai, W.; Yager, K. G.; Ross, C. A. In Situ Characterization of the Self-Assembly of a Polystyrene-Polydimethylsiloxane Block Copolymer during Solvent Vapor Annealing. *Macromolecules* **2015**, *48* (23), 8574–8584. https://doi.org/10.1021/acs.macromol.5b02174.
(43) Batista, M. M.; Guirardello, R.; Krähenbühl, M. A. Determination of the Hansen Solubility Parameters of Vegetable Oils, Biodiesel, Diesel, and Biodiesel–Diesel Blends. *J. Am. Oil Chem. Soc. 2014 92:1* **2014**, *92* (1), 95–109. https://doi.org/10.1007/S11746-014-2575-2.
(44) HSP Basics | Practical Solubility Science | Prof Steven Abbott https://www.stevenabbott.co.uk/practical-solubility/hsp-basics.php (accessed 2022 -02 -07).
(45) Ho, D. L.; Glinka, C. J. New Insights into Hansen's Solubility Parameters. *J. Polym. Sci. Part B: Polym. Phys.* **2004**, *42* (23), 4337–4343. https://doi.org/10.1002/POLB.20283.
(46) Mieczkowski, R. Solubility Parameter Components of Some Polyols. *Eur. Polym. J.* **1991**, *27* (4–5), 377–379. https://doi.org/10.1016/0014-3057(91)90191-P.
(47) Konishi, J.; Fujita, K.; Nakanishi, K.; Hirao, K. Monolithic TiO_2 with Controlled Multiscale Porosity via a Template-Free Sol−Gel Process Accompanied by Phase Separation. *Chem. Mater.* **2006**, *18* (25), 6069–6074. https://doi.org/10.1021/cm0617485.
(48) Gunkel, I.; Gu, X.; Sun, Z.; Schaible, E.; Hexemer, A.; Russell, T. P. An in Situ GISAXS Study of Selective Solvent Vapor Annealing in Thin Block Copolymer Films: Symmetry Breaking of In-plane Sphere Order upon Deswelling. *J. Polym. Sci. Part B: Polym. Phys.* **2016**, *54* (2), 331–338. https://doi.org/10.1002/polb.23933.
(49) Mac Fhionnlaoich, N.; Qi, R.; Guldin, S. Application of the Spatial Distribution Function to Colloidal Ordering. *Langmuir* **2019**, *35* (50), 16605–16611. https://doi.org/10.1021/acs.langmuir.9b02877.
(50) Graberg, T. von; Hartmann, P.; Rein, A.; Gross, S.; Seelandt, B.; Röger, C.; Zieba, R.; Traut, A.; Wark, M.; Janek, J.; Smarsly, B. M. Mesoporous Tin-Doped Indium Oxide Thin Films: Effect of Mesostructure on Electrical Conductivity. *Sci. Technol. Adv. Mater.* **2011**, *12* (2), 025005. https://doi.org/10.1088/1468-6996/12/2/025005.

(51) Mondini, S.; Ferretti, A. M.; Puglisi, A.; Ponti, A. Pebbles and PebbleJuggler: Software for Accurate, Unbiased, and Fast Measurement and Analysis of Nanoparticle Morphology from Transmission Electron Microscopy (TEM) Micrographs. *Nanoscale* **2012**, *4* (17), 5356. https://doi.org/10.1039/c2nr31276j.